An Intelligent Time-adaptive Data-driven Method for Sensor Fault Diagnosis in Induction Motor Drive System

Bin Gou, *Member, IEEE*, Yan Xu, *Member, IEEE*, Yang Xia, Student *Member, IEEE*, Gary Wilson, and Shuyong Liu

***Abstract*—Three-phase PWM inverter fed induction motor drive system is widely applied in high power drive applications. Sensor faults are very common in the drive system which, once occur, might result in degraded system performance or even system shutdown. In order to rapidly and accurately diagnose the sensor faults, this paper proposes an intelligent time-adaptive data-driven method to identify the fault location and fault type of sensors in drive system. An emerging machine learning technology named extreme learning machine (ELM) is applied to learn the sensor fault dataset, an ensemble ELM classifier is then designed to improve diagnostic accuracy, based on which a time-adaptive fault diagnosis process is proposed to achieve a high and balanced diagnostic accuracy and speed. As a data-driven method, the proposed method only employs the phase current, DC-link voltage, and speed signals as the inputs to the ensemble ELM classifiers, and requires no additional sensors and other hardware. Simulated and experimental tests show that the proposed method can rapidly and accurately detect the fault sensor location and identify offset fault, stuck fault, and noise faults with an average diagnostic accuracy of 98% and average decision time of 10ms after the fault occurs. Moreover, such diagnosis method is robust to the fluctuation of catenary voltage and DC-link voltage, fault severity, and variation of model parameters, speed, and load.**

***Index Terms*—Fault diagnosis, Sensor fault, Three-phase inverter, Data-driven method, Time-adaptive diagnosis process.**

I. Introduction

THREE- phase PWM inverter fed induction motor drive system has been widely used in various high-power industrial systems. Generally, in these drives, closed-loop controls are used to achieve high drive performances. In the integrated closed-loop, DC-link voltage, three-phase currents, and rotor position signals are required to generate command signals of the power converter, as shown in Fig. 1. However, sensors in the drive systems are prone to faults due to device aging, mechanical vibration, humidity environment, and surrounding interference, etc. [1]. Once occurred, the erroneous feedbacks due to sensor fault could result in degraded control performance or even shutdown of the drive system.

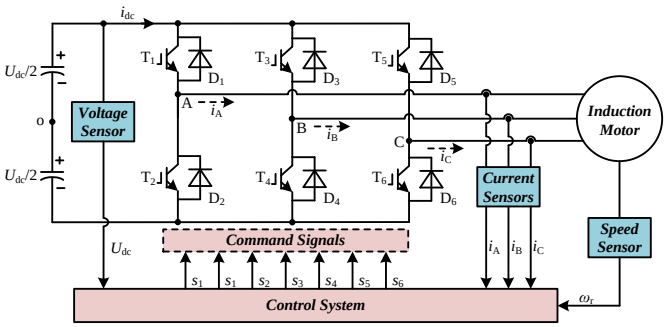

Fig. 1. The structure of three-phase inverter fed induction motor drive system.

The typical fault modes of the sensor can be broadly classified as offset fault, stuck fault, and noise fault, according to the measurement results [2]. To diagnose the sensor faults, the methods can be categorized as model-based, signal-based, and data-driven methods [3], which are reviewed as follows.

For model-based methods, the practical systems are modeled by either physical principles or system identification methods. These model-based methods aim to monitor and evaluate the system residuals which are generated by comparing the measured outputs of the practical systems and the model-generated outputs. State observer-based approach is one of the representative model-based diagnosis methods, including Luenberger observer, adaptive observer, sliding mode observer, extended Kalman filters (EKF), etc. In [4] and [5], a Luenberger observer and sliding mode observer of catenary current and DC-link voltage are designed to generate residuals to detect sensor faults for a single-phase PWM rectifier in high-speed railway electric traction system, respectively. In [6], a full-order Luenberger observer with an adaptive threshold is designed to detect the rotor-position-sensor fault of permanent magnet synchronous motor (PMSM) drives in an electro-mechanical brake. In [7], an EKF is designed to estimate the

Manuscript received June 30, 2018; revised October 7, 2018; accepted October 24, 2018.

Bin Gou, is with the Rolls-Royce @ NTU Corporate Lab, Nanyang Technological University, Singapore. (e-mail: goubin@ntu.edu.sg).

Yan Xu and Yang Xia are with the School of Electrical and Electronic Engineering, Nanyang Technological University, Singapore (+65 67904508, e-mail: xuyan@ ntu.edu.sg and xiay0020@e.ntu.edu.sg).

Gary Wilson and Shuyong Liu are with Electrical Capability Group of Rolls-Royce Singapore. (e-mail: Gary.Wilson5@Rolls-Royce.com and Shuyong.Liu@Rolls-Royce.com).

rotor speed and phase currents of PMSM drive. The faulty sensors are diagnosed by comparing the measured and EKF outputs. Model reference adaptive system based method is also effective for continuously estimating the rotor speed and phase currents [8]. A flux-linkage observer is used to estimate the current corresponding to the faulty phase in [9]. In [10], an immune system inspired mechanism is introduced to diagnose fixed value fault and gain factor fault of pitch position and speed sensors in wind turbines.

For signal-based methods, the diagnosis process is based on real-time evaluating the symptoms obtained by feature extraction. For instance, an average normalized currents method is proposed in [11] to detect the current sensor fault in PMSG drives in wind energy conversion systems. This method can only detect the faulty phase, but cannot identify the faulty types of the sensor. In [12], axes transformation and model reference adaptive system are integrated to detect the current sensors and speed sensor fault in induction motor drives, respectively. Gou et al. [13] developed a load currents analysis based method to distinguish the current sensor faults in three-phase voltage source inverters. It can also identify current sensor faults within one fundamental period. But the identification accuracy of fault types is sensitive to the load variation. In [14], the asymmetry between phase currents is used for detecting current sensor fault, and field and torque components of stator currents are analyzed to detect speed sensor fault in induction motor drives. This method is based on the intrinsic characteristics of field-oriented control induction motor drives. Its effectiveness is questionable when being applied to other motor control scheme, such as direct torque control and model predictive control.

Apart from the above two methodologies, based on the advancement in artificial intelligence, the data-driven method becomes a promising alternative for fault diagnosis. The data-driven method is based on extracting the mapping relationship knowledge from the fault database which can be obtained from the historical data and online monitoring data. In [15], a model-based method is extended to the data-driven method. A least-square support vector machine (LS-SVM) is used to generate system residuals, which are analyzed by discrete wavelet transform to detect the sensor fault and plant fault. The performance highly relies on the accuracy of the predictor model. Based on the similar idea, reference [16] designed a relevance vector machine predictor to evaluate the system, and principal component analysis is used to detect multifunctional self-validating sensor faults. In [2], a statistical time-domain feature extraction method is used to extracting the fault features and a support vector machine (SVM) is used for classification of sensor faults.

In general, most of the sensor fault diagnosis methods are model-based since it is fast, load independent and require no additional sensors, but its performance highly depends on the accuracy of the model and parameter estimation. However, accurate models are usually unavailable and/or their parameters are hard to estimate. The signal-based method is independent of system parameters and model, but it usually suffers from slow diagnosis speed and is highly sensitive to the system's loading condition. Compared with model- and signal-based methods, data-driven method has higher generalization capability and robustness for complex systems. But the drawbacks of the data-driven method are unsatisfactory diagnosis speed and accuracy, as well as heavy training and tuning burden. Moreover, most of sensor fault diagnosis methods did not consider the sensor fault types. In the literature, very few methods could simultaneously identify the fault location and fault type.

To overcome the inadequacies discussed above, this paper develops an intelligent time-adaptive data-driven fault diagnosis scheme for DC-link voltage sensor, phase current sensors, and speed sensor in high power drive systems. The fault types of sensors are considered as stuck, offset, and noise fault. The inputs of the data-driven model are only the voltage, current, and speed measurements, and outputs are fault location and fault type. An emerging and promising learning technology named extreme learning machine (ELM) is adopted as the classifier due to its much faster learning speed, better generalization capacity, and computationally efficient tuning mechanism [17]. In order to identify potentially inaccurate fault diagnosis results, an ensemble learning model based on a series of ELM classifiers is proposed to improve the classification accuracy and provide credibility of the outputs of classifiers. Finally, this paper designs a time-adaptive diagnosis process instead of using a fixed diagnosis cycle to balance the diagnostic accuracy and speed. After evaluating the credibility of the ensemble classifiers, the proposed diagnosis process can deliver an accurate result as early as possible.

Compared with the existing data-driven based methods which suffer from slow diagnostic speed and heavy computational burden, the proposed intelligent time-adaptive data-driven method can identify the fault location and fault type of sensor faults at a much faster speed and a higher accuracy.

II. System Description and Fault Labeling

Fig. 1 shows a typical power drive system with a two-level three-phase PWM inverter and an induction motor. Each phase leg of the inverter consists of two power switches with corresponding antiparallel connected diodes. DC-link voltage, three-phase currents, and speed sensors are implemented to accomplish the closed-loop control strategies of space vector pulse width modulation and field-oriented control for converter and induction motor, respectively.

A. Sensor Fault Definition

Fig. 1 shows a typical power drive system with a two-level three-phase PWM inverter and an induction motor. Each phase leg of the inverter consists of two power switches with corresponding antiparallel connected diodes. DC-link voltage, three-phase currents, and speed sensors are implemented to accomplish the closed-loop control strategies of space vector pulse width modulation and field-oriented control for converter and induction motor, respectively.

In general, there are three common fault types in the current sensor according to the measurement result: stuck, offset, and noise fault, which are defined as Eqs. (1) to (3), respectively.

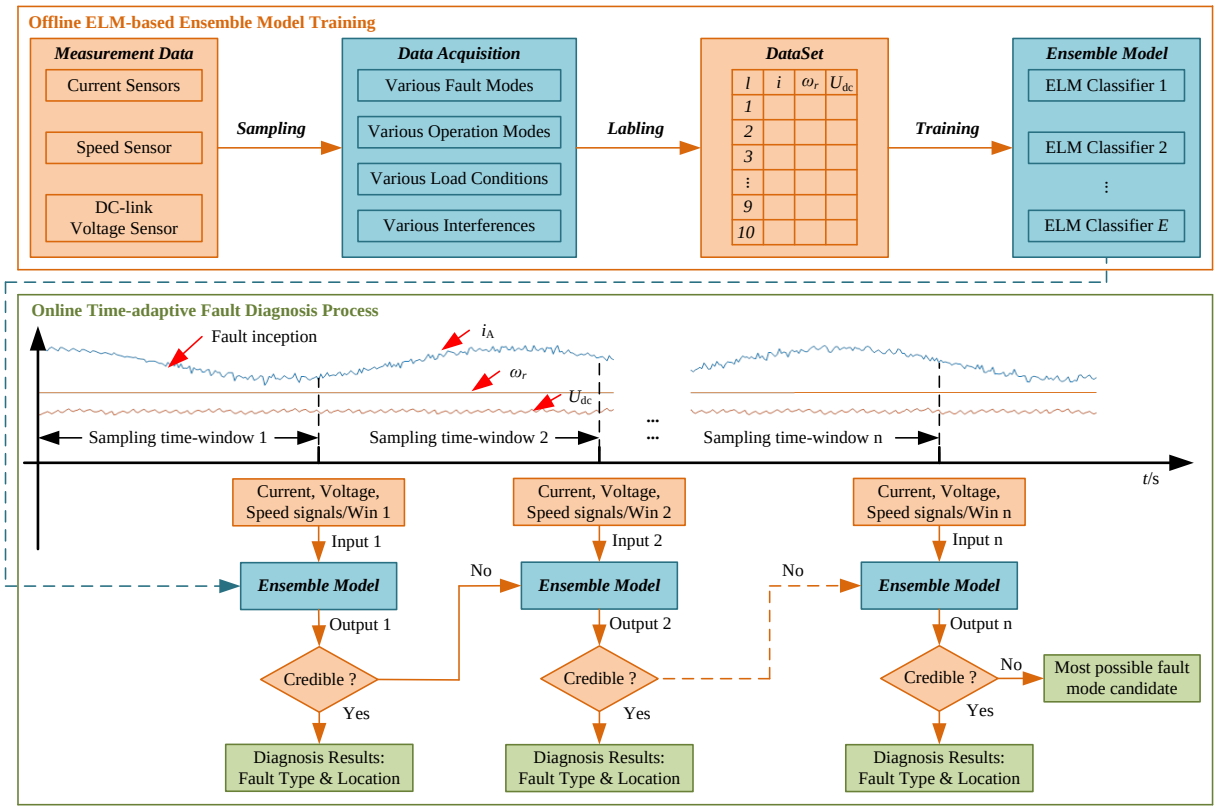

Fig. 2. The proposed fault diagnosis structure based on ensemble ELMs time-adaptive process.

$$y(t)=\begin{cases} y_{\mathrm{n}}(t), & 0\le t<t_0 \\ C_1(t), & t\ge t_0 \end{cases} \tag{1}$$

$$y(t)=\begin{cases} y_{\mathrm{n}}(t), & 0\le t<t_0 \\ y_{\mathrm{n}}(t)+C_2(t), & t\ge t_0 \end{cases} \tag{2}$$

$$y(t)=\begin{cases} y_{\mathrm{n}}(t), & 0\le t<t_0 \\ y_{\mathrm{n}}(t)+\Delta\varphi(t), & t\ge t_0 \end{cases} \tag{3}$$

where $y(t)$ is the output of the sensor, $y_{\mathrm{n}}(t)$ is the normal state output of the sensor, both $C_1(t)$ and $C_2(t)$ are DC components, $\Delta\varphi(t)$ is a zero-mean white noise Gaussian sequence, and t_0 is the fault moment of the sensor.

DC-link voltage sensor fault can reduce the speed regulation ability of motor and cause a large pulsation of speed and torque. A current sensor fault can result in imbalanced current flowing into the motor which causes overheat and fluctuations of speed and torque. Speed sensor fault repudiates the orthogonal alignment of field and torque current components in field-oriented IM drives, thereby leading to fluctuating harmonic components in speed and phase currents.

B. Labeling of Sensor Faults

Different sensor faults will result in different output signals in currents, voltage, and speed. This paper labels different faults as different numeric numbers as shown in Table I. Each label represents a fault type of sensor, for instance, "2" represents that stuck fault occurs in the current sensor of phase A.

According to Table I, there are a total 10 fault statuses of the system, including normal situation, current sensor, voltage sensor, and speed sensor faults. In order to diagnose these fault types simultaneously, this paper develops a data-driven based method to extract the mapping relationship knowledge between the inputs and outputs, where the inputs are integrated data of current, DC-link voltage, and speed signal, and output is a fault label that denotes the fault location and fault type.

TABLE I
LABELING OF SENSOR FAULTS

Fault Scenarios	Label
No Fault	1
Current Sensor of Phase A Stuck Fault	2
Current Sensor of Phase A Offset Fault	3
Current Sensor of Phase A Noise Fault	4
DC-link Voltage Sensor Stuck Fault	5
DC-link Voltage Sensor Offset Fault	6
DC-link Voltage Sensor Noise Fault	7
Speed Sensor Stuck Fault	8
Speed Sensor Offset Fault	9
Speed Sensor Noise Fault	10

III. PROPOSED METHODOLOGY

In this paper, a randomized learning technology named ELM is applied as a basic tool for extracting the mapping knowledge. Benefited from ELM's extraordinary fast learning speed and less computational burden, an ensemble-based scheme is then proposed for high diagnostic speed and accuracy. Based on the ensemble model, a time-adaptive diagnosis process is designed at last to balance the diagnostic accuracy and speed.

A. Fault Diagnosis Framework Design

The proposed fault diagnosis framework is illustrated in Fig. 2. The aim of the fault diagnosis process is to rapidly and accurately determine the output as long as the input is fed. It is worth mentioning that some research works in the literature

also apply the feature extraction and selection methods to compose or select the inputs [18]. But these data process will cost a certain time. So, this paper directly uses the system measurements as the inputs.

As shown in Fig. 2, the proposed fault diagnosis method composes of offline training and online diagnosis. Data from sensors under various fault statuses and operation conditions of drive system are collected to constitute a dataset. ELM is trained as a basic classifier to extract the mapping relationship between the trajectories and the fault statuses of system. By combining a set of individual basic ELM classifiers, an ensemble model is designed to improve the accuracy and evaluate the credibility. After that, a time-adaptive decision-making process is proposed to achieve a high and balanced diagnostic accuracy and speed.

It is important to indicate that most of the existing diagnosis methods use a fixed diagnosis time and a stationary decision process, which means the diagnosis result is either fault or normal after the diagnostic cycle. Clearly, this will not be fast enough or accurate enough since different fault with different severity may have different signatures and therefore requires different time. In this paper, a time-adaptive diagnosis process is designed to identify the sensor fault as early as possible while maintaining a high accuracy. In this process, "*credibility*" is introduced to evaluate the diagnostic decision result. If the result at first time-window is evaluated credible, the diagnosis process will stop and deliver the diagnostic result at this time-window; otherwise, the process will continue at next time-window. Owe to this time-adaptive process, the faults with distinct features can be identified earlier. While the other faults without obvious features are moved to the next time-window to utilize more information for an accurate diagnosis. As shown later in this paper, this process can improve the diagnostic accuracy without increasing much diagnostic time.

B. Extreme Learning Machine Algorithm

As a randomized learning technology, ELM was originally proposed for single hidden-layer feedforward neural networks (SLFN) and was then extended to the generalized SLFNs where the hidden layer need not be neuron alike [19]. The key is to randomly select the input weights and analytically determine the output weights. Thus, ELM has much better computational scalability, especially for huge datasets. Once proposed, ELM has received extensive interests from academic and industry.

ELM consists of three layers: input, hidden, and output layer. Given a training set $\aleph_N=\{(\mathbf{x}_j, \mathbf{t}_j)|\mathbf{x}_j\in\mathbf{R}^n, \mathbf{t}_j\in\mathbf{R}^m\}_{j=1}^N$, where $\mathbf{x}_j$ is the $n \times 1$ input vector and $\mathbf{t}_j$ is an $m \times 1$ target vector, the output function of ELM for generalized SLFNs with $\tilde{N}$ hidden nodes is

$$f_{\tilde{N}}(\mathbf{x}_j)=\sum_{i=1}^{\tilde{N}}\beta_i\cdot\vartheta(\mathbf{w}_i\cdot\mathbf{x}_j+b_i)=t_j,\ j=1,2,...,N \tag{4}$$

where ϑ is the activation function, $\mathbf{w}_i$ is the weight vector connecting the ith hidden node and the input nodes, β_i is weight vector connecting the ith hidden node and the output nodes, and b_i is the bias of the ith hidden node, $\mathbf{w}_i\cdot\mathbf{x}_j$ denotes the inner product of $\mathbf{w}_i$ and $\mathbf{x}_j$. According to ELM theory [17], (4) can be rewritten into a compact format as

$$\mathbf{H}\beta=\mathbf{T} \tag{5}$$

where $\mathbf{H}$ is the hidden layer output matrix of the network. Thus, the ELM learning process can be summarized as three steps:

Step 1: Randomly assign input weight and bias;

Step 2: Calculate the hidden layer output matrix $\mathbf{H}$;

Step 3: Calculate the output weight matrix $\beta=\mathbf{H}^{\dagger}\mathbf{T}$;

where $\mathbf{H}^{\dagger}$ is the Moore–Penrose generalized inverse of matrix $\mathbf{H}$, and can be calculated by *singular value decomposition* (SVD) for better generalization performance.

ELM is widely applied in categorical classification and numeric prediction fields in recent years [20] [21]. Since the weights are randomly assigned, ELM learning process has no time-consuming adjustment of network parameters. Compared with traditional learning algorithms, its learning speed can be thousands of times faster and requires much less computation memory, which provides a way to overcome the drawbacks of the traditional data-driven based diagnosis methods [22].

Conventional ELM is used for binary classification. But for our problem, in order to identify various sensor faults simultaneously, the ELM multiclass classification is applied.

C. Extreme Learning Machine for Multiclass Classification

According to [22], (4) can also be rewritten as

$$f_{\tilde{N}}(\mathbf{x})=\sum_{i=1}^{\tilde{N}}\beta_i h_i(\mathbf{x})=\mathbf{h}(\mathbf{x})\beta \tag{6}$$

where $\mathbf{h}(\mathbf{x})=[h_1(\mathbf{x}),...,h_{\tilde{N}}(\mathbf{x})]$ is the output vector of the hidden layer with respect to the input $\mathbf{x}$, $\beta=[\beta_1,...,\beta_{\tilde{N}}]^T$ is the vector of the output weights between the hidden layer of $\tilde{N}$ nodes. $\mathbf{h}(\mathbf{x})$ actually maps the data from the d-dimensional input space to the d-dimensional hidden-layer feature space H, and thus, $\mathbf{h}(\mathbf{x})$ is indeed a feature mapping. For the binary classification applications, the decision function of ELM is

$$f_{\tilde{N}}(\mathbf{x})=\mathrm{sign}(\mathbf{h}(\mathbf{x})\beta)\ . \tag{7}$$

As long as the dimensionality of the feature mapping (number of hidden nodes $\tilde{N}$ in a classifier) is large enough, the output of the classifier $\mathbf{h}(\mathbf{x})\beta$ can be as close to the class labels in the corresponding regions as possible.

For the binary classification case, ELM only uses a single output node, and the class label closer to the output value of ELM is chosen as the predicted class label of the input data. For the multiclass classification case, such as the fault diagnosis of sensors in this paper, there are two candidate methods:

1) Multiclass Classifier with Single Output: ELM only uses a single-output node, and among multiclass labels, the class label closer to the output value of ELM is chosen as the predicted class label of the input data. In this case, the ELM solution to the binary classification case becomes a specific case of multi-class solution. The decision function of ELM classifier is [22]

$$f(\mathbf{x})=sign(\mathbf{h}(\mathbf{x})(\frac{\mathbf{I}}{C}+\mathbf{H}\mathbf{H}^{\mathrm{T}})^{-1}\mathbf{H}^{\mathrm{T}}\mathbf{T}\ ). \tag{8}$$

where C is a user-specified parameter and provides a tradeoff between the distance of the separating margin and the training

error.

2) Multiclass Classifier with Multi-outputs: ELM uses multi-output nodes, and the index of the output node with the highest output value is chosen as the predicted class label of the input data. For instance, given a training sample $\mathbf{x}$, the output node of ELM can be computed by $\mathbf{f}(x) = [f_1(x), \ldots, f_m(x)]$, where m is the number of output nodes. Then the universal decision function of ELM classifier with multi-outputs is

$$\text{label}(x) = \arg\max_i f_i(x), \ i \in [1, \ldots, m]. \quad (9)$$

D. Credibility-oriented Ensemble Classifier

ELM has much faster-learning speed than conventional technique such as ANN, SVM, and LS-SVM [22], especially suitable for the large sized data processing since it adopts random input weights for learning. However, this randomness could make single ELM unstable and diverse in outputs. But on the other hand, the randomness also gives a chance to achieve ensemble learning to increase learning accuracy by combining a set of individual learners to make a plurality decision [20].

1) Learning process

In this paper, a set of ELM classifiers are assembled. Each ELM classifier randomly chooses the input weight and hidden nodes. Besides the sake of diversity, the single ELM classifier can compensate for each other, and the whole can reduce aggregated variance and tend to increase accuracy over the individuals [23][24].

The proposed ELM-based ensemble learning process can be described as follows:

ELM Ensemble Learning Rule

Given E single ELMs and a database of $F \times D$ size (where F and D are the total number of features and instances, respectively),

for i=1 to E:

Randomly sample d instances out of the database, $1 \le d \le D$.

Randomly assign the i-th ELM h hidden nodes and an activation function, h is within the optimal range [$h_{\min}$, $h_{\max}$], which is subject to a pre-tuning procedure).

Train this ELM and return.

End

2) Classification rule

According to the statistical classification rule of equation (9), the output is always prone to errors, which can lead to misclassification. For instance, the value of output node of ELM, $f_1(x), \ldots, f_m(x)$ could be closed to each other, when the features of two different samples are similar. This paper designs an ensemble model to simultaneously evaluate the credibility of the classification result. Firstly, the sum of the output nodes of the single classifiers is the output of the ensemble classifier. Then, the largest output node of the ensemble classifier is compared with the mean value of the individual output nodes. The classification result is evaluated as credible when the error of the largest value and mean value of the ensemble output nodes is beyond a threshold. Given all the single classification results, the ensemble classification evaluates the credibility of the classification result, described as:

ELM Ensemble Classification Rule

Given E single ELM and a database of $F \times D$ size (where F and D are the total number of features and instances, respectively),

if $\max(\sum_{k=1}^{E} \mathbf{f}_k(x)) - mean(\sum_{k=1}^{E} \mathbf{f}_k(x)) \ge T_d$

$\text{label}(x) = \arg\max_i \mathbf{f}_k(x)$, (credible sub-output)

else label(x) = 0 (incredible sub-output)

end

Where $\mathbf{f}_k(x) = [f_{k1}(x), \ldots, f_{km}(x)]$, i=1, 2, … , m; k is the k-th ELM classifier, ($1 \le k \le E$); T_d is a threshold to evaluate the credibility of the classification result.

With compensation of the single ELM classifier, the accuracy of the ensemble classifier could be improved. Besides, with the ensemble decision-making rule, the classifier is able to identify the incredible classification results that should not be adopted. Thus, the risk of misclassification can be effectively reduced.

E. Time-adaptive Fault Diagnosis Process

The model-based method has the advantage of fast diagnostic speed since the diagnosis process is essentially an adaptive procedure. Based on evaluating the system residuals online, faults with evident signatures can be detected earlier, while faults with minor signatures need more time and information to be accurately diagnosed. Traditionally, for the signal-based method and data-driven method, the diagnostic decision time is generally one fundamental period. After the decision time, there must be a diagnosis result, no matter accurate or not. This diagnosis process is less efficient when dealing with various fault types of power drive system.

Inspired by the diagnosis process of model-based method, this paper designs a time-adaptive diagnosis process to balance between diagnostic accuracy and speed, illustrated as Fig. 2.

As shown in the online diagnosis process part of Fig. 2, at each time-window, the integrated current, voltage, and speed trajectories are fed to the ensemble ELM classifier. If the classification result by ensemble ELM classifier is evaluated as "*credible*" using the method proposed in Section III-D, the diagnosis process will stop and deliver the diagnostic result at the current sampling time-window; otherwise, the classification will continue to the next time-window, and the newly received measurement data will be integrated into the inputs for classification again. With more system dynamic trajectories, the accumulated classification accuracy tends to be higher. This time-adaptive procedure will continue until a credible classification output is obtained or the maximum allowable decision window is reached. Evidently, based on such a time-adaptive process, an accurate diagnostic result can be obtained as early as possible.

IV. Simulation and Experimental Validations

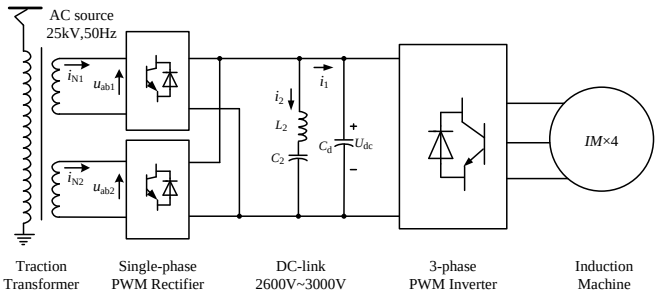

Fig. 3. The strucutre of the AC-DC-AC railway traction system.

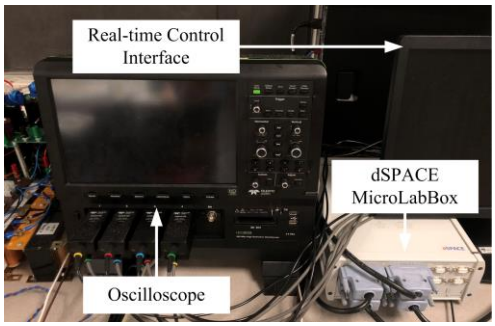

Fig. 4. Experimental setup.

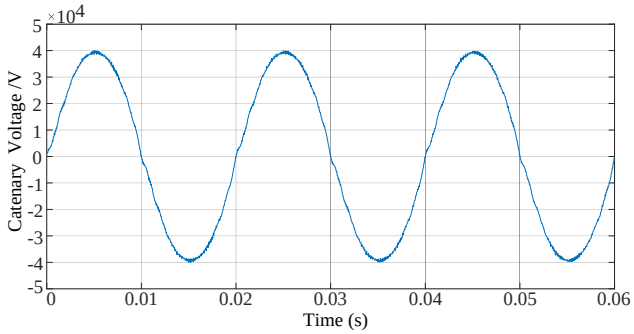

Fig. 5. Catenary voltage data sampled from real high-speed train.

The proposed intelligent time-adaptive data-driven fault diagnosis method is verified on the AC-DC-AC electrical railway traction test system. As shown in Fig. 3, the test system consists of catenary, transformer, single phase PWM rectifier, three-phase PWM inverter, and induction motor.

A. Data Acquisition

According to Table I, there are a total of 10 fault statuses. It is impractical to acquire a large volume of data with experimental measurement under all these fault statuses and load conditions. Thus, the data is collected by combining the experimental and simulation tool in this paper. In practice, the historical fault recording data can also be combined together in the training dataset.

The simulation model of the drive system is performed by using MATLAB/Simulink software. The experimental platform comprises a controller to generate command signals of IGBTs, a dSPACE MicroLabBox, and a computer as a real-time control interface, as shown in Fig. 4. The hardware circuits of the traction drive system (as shown in Fig. 3) and sensors are simulated in the dSPACE simulator. The sensor faults are simulated according to Eqs. (1) to (3). Both simulation and experimental parameters given in Table II and Table III are the same and comply with the high-speed train

TABLE II
PARAMETERS OF CONVERTER

Parameter	Symbol	Value
RMS grid voltage	u_N	1550V
Traction winding leakage inductor	L_N	2.3mH
Traction winding resistor	R_N	0.068Ω
DC-link voltage	U_{dc}	2700V-3600V
DC-link capacitor	C_d	3mF
Series resonant circuit inductor	L_2	0.603mH
Series resonant circuit capacitor	C_2	4.56mF
Rectifier switching frequency	f_R	350Hz
Highest inverter switching frequency	f_i	500Hz

TABLE III
PARAMETERS OF INDUCTION MOTOR

Parameter	Symbol	Value
Stator resistance	R_s	0.1065Ω
Stator leakage inductance	L_{ls}	1.31mH
Rotor resistance	R_r	0.0663Ω
Rotor leakage inductance	L_{lr}	1.93mH
Mutual inductance	L_m	53.6mH
Rated voltage	U_{rate}	2700kV
Rated speed	n_{rate}	4100(r/min)
Rated frequency	f_{srate}	138Hz
Rated output power	P_{rate}	562kW
Rated slip frequency	s_{rate}	0.04
Number of the pole pairs	np	2
Moment of inertia	J	100 kg·m2

named CRH3 (China Railway High-speed). The load torque is determined by the speed of the train since air resistance is the most important factor of the load for a high-speed train and speed dependent. The air resistance, w_0 (N), is described as,

$$w_0 = 0.2859 + 0.00321v + 0.000125v^2 \qquad (10)$$

where v is the speed of the train, km/h.

In order to ensure a unity power factor operation and DC-link voltage regulation, a proportional integrator (PI) controller in the external control loop and a proportional-resonant (PR) controller in the inner loop control are adopted in the rectifier-side control. Space vector pulse width modulation and indirect field-oriented control are applied in the inverter-side control.

To examine the reliability of the proposed diagnosis method under various operation conditions, catenary voltage, DC-link voltage ripple and harmonics, speed and load variation are all considered. Thus, the phase currents, DC voltage, and speed sensor signals of the 10 fault statuses are collected, where the amplitude of the third order harmonic in catenary voltage varies from 100V to 5 kV with the interval of 100V, the reference voltage of DC-link varies from 2.9 to 3.1 kV with the interval of 4 V, the reference speed varies from 2 to 100 rad/s with the interval of 2 rad/s. Besides, the catenary voltage sampled from the actual high-speed train is applied to the drive system to collect more practical operational data, as shown in Fig. 5.

Meanwhile, the experimental data are collected under the same operation conditions, but the interval is 10 times larger than simulation data to save the experimental data acquisition time. Moreover, data from the regenerative braking mode of the drive system are also collected to verify the effectiveness of the proposed diagnosis method. The control and signal sampling frequency for both experiment and simulation are 25 kHz and 5 kHz, respectively. Thus, the database of the total 10 fault statuses can be summarized in Table IV.

TABLE IV
DATA ACQUISITION UNDER DIFFERENT FAULT STATUSES AND OPERATION CONDITIONS

	Catenary harmonic voltage	Reference voltage of DC-link	Reference speed	Traction mode	Regenerative braking mode
Simulation data	50 (100 V : 5 kV/100 V)	50 (2.9 : 3.1 kV/4 V)	50 (2 : 100/2 rad/s)	1500 sets	1500 sets
Experimental data	5 (1 kV : 5 kV/1000 V)	5 (2.9 : 3.1 kV/40 V)	5 (20: 100/20 rad/s)	150 sets	150 sets

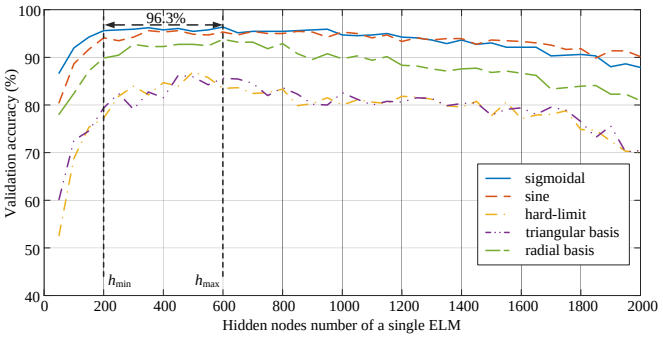

Fig. 6. Single ELM hidden nodes versus validation accuracy (%).

The database is acquired by integrating the experimental data and simulated data. A total of 3300 data samples for ELM are obtained. In the test, 20% of the dataset is randomly selected as testing data and the remaining serves as training data. Thus, there are 660 testing and 2,640 training instances for each ELM to identify the sensor faults.

B. Parameters Tuning

It should be noted that the ELM has very few user-defined parameters. Only the activation function and the hidden node number should be well-tuned. In this paper, [h_{min}, h_{max}] is the optimal hidden nodes range for single ELMs which is selected at the highest validation accuracy range. For activation function, five initial activation functions are considered, namely, 'sine', 'sigmoidal', 'hard-limit', 'triangular basis' and 'radial basis', where the highest accuracy by the activation function is selected. The validation result is illustrated in Fig. 6, where testing data is randomly selected from the 20% of the dataset and training data is the remaining instances of the dataset. It is clear that the validation accuracy is the highest when activation function is set as 'sigmoidal'. [h_{min}, h_{max}] can accordingly be set as [200, 600], where the single ELM achieves the highest accuracy of 96.3 %. It is worth mentioning that the more hidden nodes, the more training time is needed.

Then, the ensemble ELM classification model is composed. The threshold T_d is a tradeoff between the diagnostic accuracy and time. The bigger T_d may lead to higher credibility and higher diagnostic accuracy, but longer diagnostic time since more incredible sub-outputs are moved to the next time-window to utilize more information to get a higher credibility and avoid false diagnosis. In the test, the sample data of each time-window, the number of ensemble classifier, E, and classification threshold, T_d, are set as 40, 200 and 280, respectively, according to a tradeoff between the classification efficiency against the misclassified rate. Since the sampling frequency is 5 kHz, the duration time for each time-window is 8ms.

C. Diagnosis Results Analysis

The diagnosis results are summarized as Table V, where W_i is the ith time-window, $U(W_i)$ and $C(W_i)$ are the number of unclassified and classified instances during the current time-window, respectively; $C(W)$ is the total number of accumulative classified instances; $M(W_i)$ and $M(W)$ are the current and accumulative number of misclassified instances during the time-window; $A(W_i)$ and $A(W)$ are the current and accumulative accuracy of the time-window, respectively, calculated as

$$A(W_i) = [C(W_i) - M(W_i)] / C(W_i) \quad (11)$$

$$A(W) = [C(W) - M(W)] / C(W) \quad (12)$$

TABLE V
TEST RESULTS OF THE PROPOSED METHOD

W_i	$U(W_i)$	$C(W_i)$	$C(W)$	$M(W_i)$	$M(W)$	$A(W_i)$	$A(W)$
0	660	-	-	-	-	-	-
1	60	600	600	6	6	99.0%	99.0%
2	38	22	622	1	7	95.5%	98.9%
3	26	12	634	0	7	100%	98.9%
4	21	5	639	0	7	100%	98.9%
5	1	20	659	6	13	70.0%	98.0%

TABLE VI
TEST RESULTS OF SPEED VARIATION TRANSIENT

W_i	$U(W_i)$	$C(W_i)$	$C(W)$	$M(W_i)$	$M(W)$	$A(W_i)$	$A(W)$
0	760	-	-	-	-	-	-
1	60	700	700	7	7	99.0%	99.0%
2	8	52	752	7	14	86.5%	98.1%
3	7	1	753	0	7	100%	98.2%
4	5	2	755	0	7	100%	98.2%
5	0	5	760	1	13	80.0%	98.0%

TABLE VII
TEST RESULTS OF DIFFERENT FAULT SEVERITY

W_i	$U(W_i)$	$C(W_i)$	$C(W)$	$M(W_i)$	$M(W)$	$A(W_i)$	$A(W)$
0	800	-	-	-	-	-	-
1	70	730	730	3	3	99.6%	99.6%
2	41	29	759	2	5	93.1%	99.3%
3	25	16	775	1	6	93.8%	99.2%
4	8	17	792	1	7	94.1%	99.1%
5	1	7	799	3	10	57.1%	98.7%

According to Table V, 600 out of 660 instances are "credibly" classified at the first time-window, where only 6 instances are misclassified. The accuracy is as high as 99.0%. The remaining 60 unclassified instances, i.e., evaluated as "*incredible*" outputs, move to the second time-window, where 22 of them are classified with only 1 instance being misclassified. The accuracy of the second time-window is as high as 95.5%. The remaining 38 unclassified instances move to the third time-window, where 12 of them got classified with the accuracy of 100%. This proceeds until the maximum allowable response window (5 time-windows). After the fifth time- window, there is still 1 instance unclassified. The highest possible classification results will be exported for the unclassified instances with the index of the maximum of the output node, to provide reasonable maintenance suggestions.

For a general estimation of the response speed and accuracy of the proposed method, the average response time (ART) and average diagnostic accuracy (ADA) can be calculated as,

$$\mathrm{ART} = \sum_{i=1}^{n}[T_i \times C(\mathrm{W}_i)] / \sum_{i=1}^{n} C(\mathrm{W}_i) \tag{13}$$

$$\mathrm{ADA} = \sum_{i=1}^{n}[C(\mathrm{W}_i) \times A(\mathrm{W}_i)] / \sum_{i=1}^{n} C(\mathrm{W}_i) \tag{14}$$

where n is the total number of the maximum allowable time-window, which is 5 in this test.

According to equation (13) and (14), the proposed time-adaptive data-driven diagnosis method can identify the stuck fault, offset fault, and noise fault for phase current sensor, DC-link voltage sensor, and speed sensor, with the average accuracy of 98.0% and average response time of 9.71ms.

D. Speed Variation Transient and Fault Severity Test

In order to further verify the proposed diagnosis method in the situations of speed variation transient and different fault severity degrees, more tests are completed. Data from constant speed variated to different speed transient level and different fault severity of all fault types are collected. The test results are summarized in Table VI and Table VII. The average diagnosis accuracies are 98.0% (8.84ms) and 98.75% (9.40ms) in the speed variation transient test and fault severity test. It can be seen that the proposed data-driven diagnosis method can accurately identify the sensor faults, even under the conditions of speed variation transient and different fault severity.

E. Real-time Hardware-in-loop Verification

To verify the online applicability of the proposed method, the real-time hardware-in-loop experimental test is also performed. Fig. 7 shows the experimental measurements in normal condition, where Ch1 trace is the stator current of phase A; Ch2 trace is the DC-link voltage signal; Ch3 trace is the speed signal of induction motor; and Ch4 trace is the fault diagnosis flag. As shown in Fig. 7, the induction motor started at the moment of t_0, begins to brake at t_1, and works as regenerative braking mode after t_2. It is clear that there is no misdiagnosis, regardless of the operation mode of the induction motor and the fluctuation of the DC-link voltage.

The experimentally measured results when the current sensor of phase A is in the offset fault are shown in Fig. 8. The offset fault is introduced at t_1, leading to a DC offset component in the current of phase A and a fluctuation in DC-link voltage signal. The fault diagnosis flag (Ch4) is changed to 3 from 1 at t_2, which indicates offset fault occurs in the current sensor of phase A according to Table I. Fig. 9 illustrates the measurement results when a stuck fault occurs in DC-link voltage sensor. The output of the sensor is kept at the reference voltage, i.e., 3000 V. Thus, there are no distinct effects on the current and speed of induction motor, but the system loses the ability of DC-link voltage control. Note that the sensor faults can be identified within 10ms. Except for the 8ms sampling-window time, the online computation time is around 2ms.

In order to verify the transient performance of the proposed data-driven method, the test of traction torque variation transient is demonstrated in Fig. 10. The reference traction torque is changed from 3000N·m to 2000N·m at the moment of t_0. The stuck fault is introduced to the current sensor at the

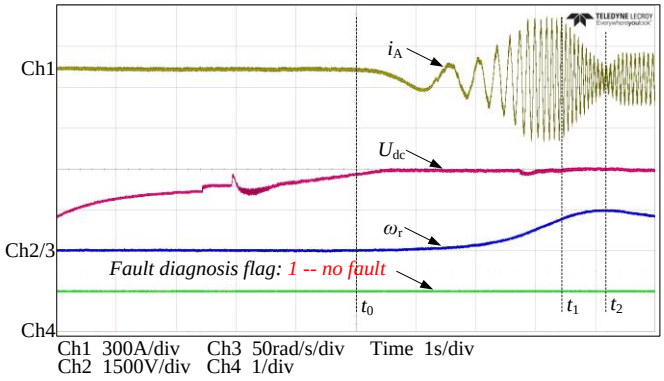

Fig. 7. Experimentally measured results in the normal condition (i_A/A, U_{dc}/V, ω_r/ rad/s).

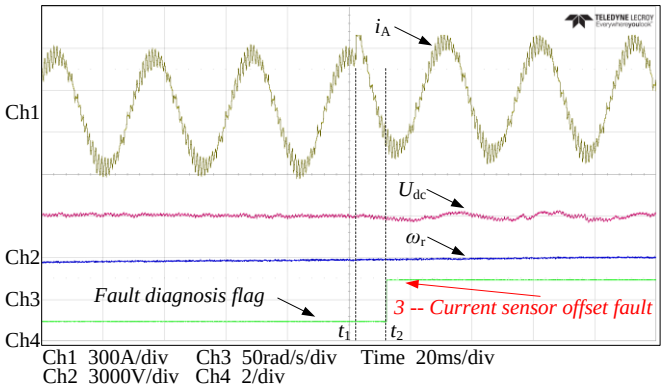

Fig. 8. Experimentally measured results when current sensor is in offset fault (i_A/A, U_{dc}/V, ω_r/ rad/s).

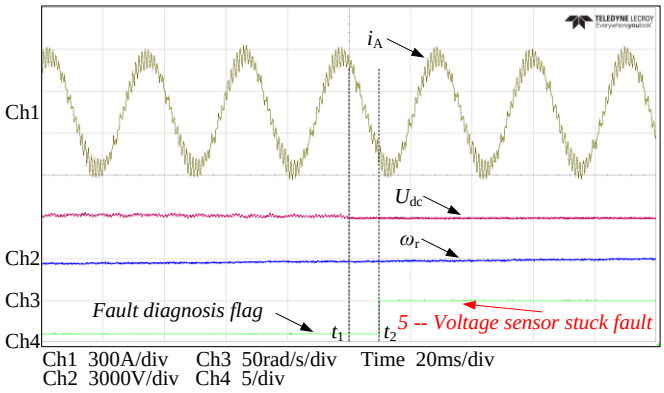

Fig. 9. Experimentally measured results when DC-link voltage sensor is in stuck fault (i_A/A, U_{dc}/V, ω_r/ rad/s).

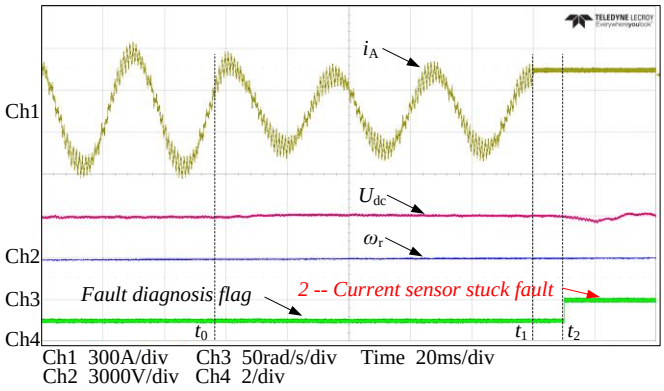

Fig. 10. Experimentally measured results when current sensor is in stuck fault under traction torque variation transient condition (i_A/A, U_{dc}/V, ω_r/ rad/s).

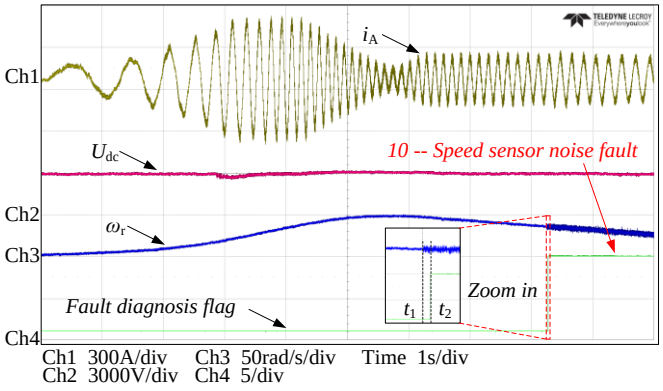

Fig. 11. Experimentally measured results when speed sensor is with a noise fault under regenerative braking mode (i_A/A, U_{dc}/V, ω_r/ rad/s).

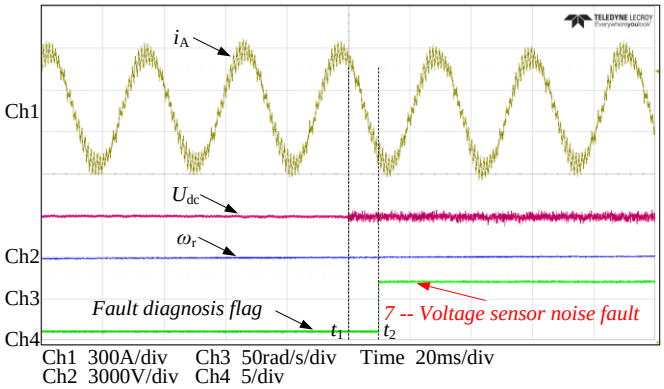

(a)

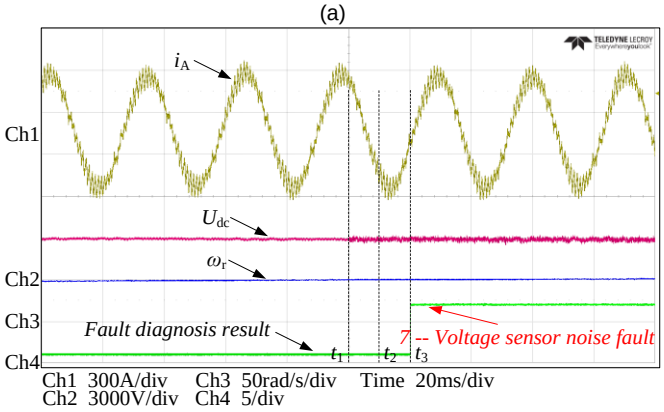

(b)

Fig. 12 Experimentally measured results when DC-link voltage sensor is with a noise fault with different severity: the noise power $\Delta\varphi_a(t)$ in (a) is four times bigger than $\Delta\varphi_b(t)$ in (b).

moment of t_1, and the diagnosis result is accurately carried out at the moment of t_2 before the big fluctuation of DC-link voltage. During the process of the action torque variation transient, there is no misdiagnosis. Fig. 8 and Fig. 10 show that the offset fault and stuck fault of the sensor have a relatively larger impact on the drive system. Both of them can result in large fluctuation of the DC-link voltage as the fault propagation. But the proposed data-driven method can timely distinguish the fault types before the fluctuation of the DC-link voltage, which provides enough time to isolate the fault and protect the drive system. Moreover, the regenerative braking mode is also a load condition of the traction drive system. The regenerative braking experimental test result illustrated in Fig. 11, shows that the proposed diagnosis method can also accurately identify the fault type even under regenerative braking mode.

The designed intelligent time-adaptive process can balance the tradeoff between the diagnostic accuracy and time, which is demonstrated by the fault severity test, presented in Fig. 12. In Fig. 12, the amplitude of noise power in the DC-link voltage signal in Fig. 12(a) is set as four times bigger than that of Fig. 12(b). Thus, the fault severity of Fig. 12 (a) is larger than that of Fig. 12 (b), which can be shown in the DC-link voltage signal, U_{dc}. In Fig. 12 (a), the classification result by ensemble ELM classifier is evaluated as "*credible*" using the method proposed in Section III-D, the diagnosis process will stop and deliver the diagnosis result after the current sampling time-window, at the moment of t_2. In Fig. 12 (b), the classification result is evaluated as "*incredible*" at the moment of t_2. And the diagnosis process continues to the next time-window to gather more measurement data. After the second time-window, the DC-link voltage sensor fault is accurately identified at the moment of t_3. Owe to this time-adaptive process, the faults with distinct features can be identified earlier. While the other faults without obvious features are moved to the next time-window to utilize more information to avoid false diagnosis.

V. Conclusion

An intelligent time-adaptive ensemble ELM based data-driven fault diagnosis method for sensors in power drive systems is proposed in this paper. The ELM algorithm is used to train and learn the faulty dataset, the ensemble ELM classifiers are proposed to increase diagnostic accuracy, and a time-adaptive fault diagnosis process is designed to better balance the tradeoff between diagnostic accuracy and speed. Phase current, DC-link voltage, and speed signals are directly used as inputs for the ELM classifier to save the time of feature extraction and selection. The proposed method can identify the stuck fault, offset fault, and noise fault of phase current, DC-link voltage, and speed sensor with a high average diagnostic accuracy in the average time of 9.71ms. Real-time hardware-in-loop test results also indicate that the proposed method can diagnose sensor faults accurately within 10ms. Moreover, the proposed data-driven diagnosis method benefits from the high expandability of other faults in the system, as long as the fault data is collected which is advantageous than model-based and signal-based method.

References

[1] G. A. Capolino, J. A. Antonino-Daviu, and M. Riera-Guasp, "Modern diagnostics techniques for electrical machines, power electronics, and drives," *IEEE Trans. Ind. Electron.*, vol. 62, no. 3, pp. 1738–1745, Mar. 2015.

[2] S. U. Jan, Y. D. Lee, J. Shin, and I. Koo, "Sensor fault classification based on support vector machine and statistical time-domain features," *IEEE Access*, vol.5, pp. 8682–8690, Jun. 2017.

[3] X. Dai and Z. Gao, "From model, signal to knowledge: A data-driven perspective of fault detection and diagnosis," *IEEE Trans. Ind. Informat.*, vol. 9, no. 4, pp. 2226–2238, Nov. 2013.

[4] A. B. Youssef, S. K. El Khil, and I. Slama-Belkhodja, "State observer-based sensor fault detection and isolation, and fault tolerant control of a single-phase PWM rectifier for electric railway traction," *IEEE Trans. Power Electron.*, vol. 28, no. 12, pp. 5842–5853, Dec. 2013.

[5] J. Xia, Y. Guo, B. Dai, and X. Zhang, "Sensor fault diagnosis and system reconfiguration approach for an electric traction PWM rectifier based on

sliding mode observer," *IEEE Trans. Ind. Appl.*, vol. 53, no. 5, pp. 4768–4778, Sept./Oct. 2017.
[6] C. Choi, K. Lee, and W. Lee, "Observer-based phase-shift fault detection using adaptive threshold for rotor position sensor of permanent-magnet synchronous machine drives in electromechanical brake," *IEEE Trans. Ind. Electron.*, vol. 62, no. 3, pp. 1964–1974, Mar. 2015.
[7] G. H. B. Foo, X. Zhang, and D. M. Vilathgamuwa, "A sensor fault detection and isolation method in interior permanent-magnet synchronous motor drives based on an extended Kalman filter," *IEEE Trans. Ind. Electron.*, vol. 60, no. 8, pp. 3485–3495, Aug. 2013.
[8] V. Verma, C. Chakraborty, S. Maiti, and Y. Hori, "Speed sensorless vector controlled induction motor drive using single current sensor," *IEEE Trans. Energy Convers.*, vol. 28, no. 4, pp. 938–950, Dec. 2013.
[9] M. Manohar, S. Das, "Current sensor fault-tolerant control for direct torque control of induction motor drive using flux-linkage observer," *IEEE Trans. Ind. Informat.*, vol. 13, no. 6, pp. 2824–2833, Dec. 2017.
[10] E. Alizadeh, N. Meskin, K. Khorasani, "A dendritic cell immune system inspired scheme for sensor fault detection and isolation of wind turbines," *IEEE Trans. Ind. Informat.*, vol. 14, no. 2, pp. 545–555, Feb. 2018.
[11] N. M. A. Freire, J. O. Estima, and A. J. M. Cardoso, "A new approach for current sensor fault diagnosis in PMSG drives for wind energy conversion systems," *IEEE Trans. Ind. Appl.*, vol. 50, no. 2, pp. 1206–1214, Mar./Apr. 2014.
[12] C. Chakraborty and V. Verma, "Speed and current sensor fault detection and isolation technique for induction motor drive using axes transformation," *IEEE Trans. Ind. Electron.*, vol. 62, no. 3, pp. 1943–1954, Mar. 2015.
[13] B. Gou, X. Ge, Y. Liu, and X. Feng, "Load-current-based current sensor fault diagnosis and tolerant control scheme for traction inverters," *IET Electron. Letters*, vol. 52, no. 20, pp. 1717–1719, Sept. 2016.
[14] F. R. Salmasi, "A self-healing induction motor drive with model free sensor tampering and sensor fault detection, isolation, and compensation," *IEEE Trans. Ind. Electron.*, vol. 64, no. 8, pp. 6105–6115, Aug. 2017.
[15] M. Heydarzadeh and M. Nourani, "A two-stage fault detection and isolation platform for industrial systems using residual evaluation," *IEEE Trans. Instrum. Meas.*, vol. 65, no. 10, pp. 2424–2432, Oct. 2016.
[16] Z. Shen and Q. Wang, "Failure detection, isolation, and recovery of multifunctional self-validating sensor," *IEEE Trans. Instrum. Meas.*, vol. 61, no. 12, pp. 3351–3362, Dec. 2012.
[17] G. B. Huang, Q. Y. Zhu, and C. K. Siew, "Extreme learning machine: Theory and applications," *Neurocomputing*, no. 70, pp. 489–501, May 2006.
[18] B. Cai, Y. Zhao, H. Liu, and M. Xie, "A data-driven fault diagnosis methodology in three-phase inverters for PMSM drive systems," *IEEE Trans. Power Electron.*, vol. 32, no. 7, pp. 5590–5600, Jul. 2017.
[19] G. B. Huang and L. Chen, "Enhanced random search based incremental extreme learning machine," *Neurocomputing*, vol. 71, no. 16–18, pp. 3460–3468, Oct. 2008.
[20] Y. Xu, Z.Y. Dong, J. Zhao, P. Zhang, and K.P. Wong, "A reliable intelligent system for real-time dynamic security assessment of power systems," *IEEE Trans. Power Syst.*, vol. 27, no. 3, pp. 1253–1263, Aug. 2012.
[21] R. Zhang, Y. Xu, Z. Y. Dong, and K. P. Wong, "Post-disturbance transient stability assessment of power systems by a self-adaptive intelligent system," *IET Gener. Transm. Distrib.*, vol. 9, no. 3, pp. 296–305, Feb. 2015.
[22] G. B. Huang, H. Zhou, X. Ding, and R. Zhang, "Extreme learning machine for regression and multiclass classification," *IEEE Trans. Syst. Man., Cybern. B, Cybern.*, vol. 42, no. 2, pp. 513–529, Apr. 2012.
[23] L. K. Hansen and P. Salamon, "Neural network ensemble," *IEEE Trans. Pattern Anal. Mach. Intell.*, vol. 12, no. 10, pp. 993–1001, Oct. 1990.
[24] L. Breiman, "Random forests," *Mach. Learn.*, vol. 45, pp. 5–32, 2001.

Bin Gou (S'14–M'17) received the B.E. and Ph.D. degrees in electrical engineering from Southwest Jiaotong University, Chengdu, China, in 2010 and 2016. He is currently a Research Fellow in the Rolls-Royce @ NTU Corporate Lab, Nanyang Technological University, Singapore.

His research interests include data-analytics for fault diagnosis and health management of power drive system.

Yan Xu (S'10-M'13) received the B.E. and M.E degrees from South China University of Technology, Guangzhou, China in 2008 and 2011, respectively, and the Ph.D. degree from The University of Newcastle, Australia, in 2013. He is now the Nanyang Assistant Professor with the School of Electrical and Electronic Engineering, Nanyang Technological University, Singapore.

His research interests include power system stability and control, microgrid and multi-energy system, and data-analytics for smart grids.

Yang Xia (S'18) received his B. E. degree from Xi'an Jiaotong University, Xi'an, China in 2017. He is currently working toward the M. E. degree at Nanyang Technological University.

His research interests include fault diagnosis and fault tolerant-control in power electronic devices.

Gary Wilson is a Principal Technologist with the Electrical Capability Group of Rolls-Royce Singapore. He has worked with the company for 4 years and he leads its research and technology development for marine electrical and control systems. He holds B.Eng. and M.Sc. degrees in Electronics and Electrical Engineering. He started his career in England as a graduate trainee with BAE Systems Submarines before joining Lloyd's Register, where he spent four years developing requirements for its electrical and control systems rules for ships. He then left Lloyd's Register and spent 2.5 years in Perth, Australia, working on mining and oil and gas projects before moving to Singapore.

His current research focus includes electrical ship power system design, development of energy storage systems and control and technologies for autonomous systems.

Shuyong Liu received the B.E. from Huazhong University of Science and Technology in 2000 and Ph.D. degree from Nanyang Technological University in 2008. He is currently with the Electrical Capability Group of Rolls-Royce Singapore.

His research interests include the intelligent fault diagnosis of electrical ship power system for unmanned ship, intelligent control system for microgrids.